14 Quantifying the Spatio-seasonal Water Balance and Land Surface Temperature Interface in Chandrabhaga River Basin, Eastern India

Susanta Mahato and Swades Pal

Abstract

Seasonal water scarcity and thermal uncomfortability in the rural environment are the increasing challenges in the growingly populated Chandrabhaga river basin area of Chottanagpur plateau fringe area. The present work, therefore, intends to investigate spatio-seasonal pattern of water balance and temperature as well as their interlinkages. High degree of spatio-seasonal variation in water balance and the land surface temperature is clearly recognized. Water deficit state is identified in seven Summer and Winter months (maximum 150.59 mm in April) and surplus state in the five monsoon months (310.81 mm in September). Upper and middle catchments are sensitive to water deficit (18.83–150.59 mm) and it withstands against multi-cropping and enhances land surface temperature (LST). LST is high (30–41 °C) in the areas prone to water deficit and it is quite less in the surplus areas. The spatial correlation coefficient between water deficit and LST is −0.2366 and it is 0.1921 between water surplus and LST and these are significant at 0.05 level of significance. It clearly establishes the linkages between water balance state and LST.

Keywords

Water balance · Water deficit or surplus · Spatio-seasonal variation of water balance · Land surface temperature (LST) · Interlinkage between water balance and LST

14.1 Introduction

In the Developing countries, about 90% of freshwater is used for agriculture purposes (Shiklomanov 2000; Perea et al. 2016) and about 70% of people rely on agriculture (Meena and Bisht 2017). In semi-arid regions it causes extra burden on natural storage units (Krol and Bronstert 2007; Yadav and Lal 2018). As consequence of this practice further water deficit, soil moisture deficit, etc. are becoming very usual (Shao et al. 2009; Vero et al. 2014; Zandalinas et al. 2016; Mohanty et al. 2017). Some areas, especially Indian subcontinent suffer from the skewed nature of annual rainfall distribution and evapotranspiration. Thus, growing need but increasing scarcity of such precious and irreplaceable resources is, in fact, an impending concern to them (Wada et al. 2012; Rohde et al. 2015). As the largest consumer of

S. Mahato
Special Centre for Disaster Research (SCDR), Jawaharlal Nehru University, New Delhi 110067, India
e-mail: susantamahato@jnu.ac.in

S. Pal (✉)
Department of Geography, University of Gour Banga, Malda 732103, India
e-mail: swadespal2017@gmail.com

S. Mandal et al. (eds.), *Applied Geomorphology and Contemporary Issues*, Geography of the Physical Environment, https://doi.org/10.1007/978-3-031-04532-5_14

fresh water and groundwater in the world, India withdraws 250 km^3 per year (Jha 2013). This amount considers the query how to be managed such growing need for water for agriculture and other sectors. Then how could drinking water be secured for the future? To understand the principal source of water, it is highly essential to consider the rainfall regime. Spatial skewness of rainfall distribution, loss of water through evapotranspiration, runoff, etc. are also essential while dealing with water balance, surplus, or deficit of water over space. Without having any major project for rainwater harvesting, a major portion of rainfall during monsoon months (June to October) is wasted. If some parts of water flow could be arrested seasonal rainfall deficit in non-monsoon seasons to some extent could be managed (Surendran et al. 2015; Mooley and Parthasarathy 1984; Yaduvanshi and Ranade 2017). Moreover, seasonal soil moisture drought is withstanding against the multi-cropping state of many parts of the country (Thober et al. 2015; Zhang et al. 2017) and as a consequence of this either people compel to grow some inferior crops or remain seasonally fallow. In India, large semi-arid tracts including parts of Central India, Western India, and Southern India fall under this tract where this problem is very prominent (Mishra et al. 2014; Sathyanadh et al. 2016). In a word, the scientific study of water balance is highly necessary for effective decision-making of water uses in progressive sectors (Khalaf and Donoghue 2012). For the hydrological cycle and water management, the replenishment rate of groundwater resources plays a key component. Seasonal or perennial water balance deficit may enhance land surface temperature (LST). Assuming this fact the present work started an investigation on the specific relation between water balance deficit and positive temperature anomaly on spatio-seasonal scale. A good number of works highlighted change in land surface temperature in relation to shift of land use/land cover (LU/LC) (Pal and Ziaul 2017; Ziaul and Pal 2016; Jafari and Hasheminasab 2017; Metz et al. 2017) highlighted increase of urban built-up land is caused for enhancing LST. González et al. (2015) and Deo and Şahin (2017) documented that abolishing water bodies, shallowing water bodies, replacing water bodies with other land uses are responsible for rising temperatures. Pal and Ziaul (2017) reported that canopy density is negatively related to LST. But the present interest of study, i.e., role of the water balance on LST is almost unexplored.

In some recent research, remote sensing (RS) and geographical information system (GIS) has contributed a major role in providing information for water resource studies and LST. Some of the eminent scholars successfully explored water balance status, and LST pattern over space using these RS and GIS techniques. Soil moisture balance study by Crosbie et al. (2015), González-Rojí et al. (2018), Hu et al. (2015), water balance study by Bastiaanssen et al. (2005), Hassan-Esfahani et al. (2015), Saiter et al. (2016) are very well known. Spatio-temporal temperature extraction from multi-temporal satellite images is well studied by Lee et al. (2012), Siu and Hart (2013), Jiang and Weng (2017), and Yao et al. (2018) for different urban sectors. But linkages between water balance and LST are still to be investigated. Therefore, the present work focused on calculating water balance by incorporating frequently used parameters like rainfall, evapotranspiration, and runoff on spatio-seasonal scale in the Chandrabhaga river basin of Eastern India and tried to find out the influence of the surplus or deficit water balance on LST.

The Chandrabhaga river basin (area: 119.34 km^2) is located over the Chattanagpur plateau fringe of Rarh tract of Jharkhand and West Bengal (Bagchi and Mukerjee 1983). Geologically 60% of the basin area lies in the upper catchment which is composed of granitic-gneissic rock of Pleistocene age (50 lakh years old) overlain by coarse-grain lateritic soil and 30% of the area at the lower catchment is made with newer alluvium of the Holocene period (Fig. 14.1) (GSI 1985). Coarse-grain lateritic soil with high ferrous and silica content contents insists high range of temperature. Most part of the basin area is dominated by agricultural land with poor qualities of soil fertility and soil moisture (during pre-monsoon 8–11%). The climate of this region is characterized by sub-

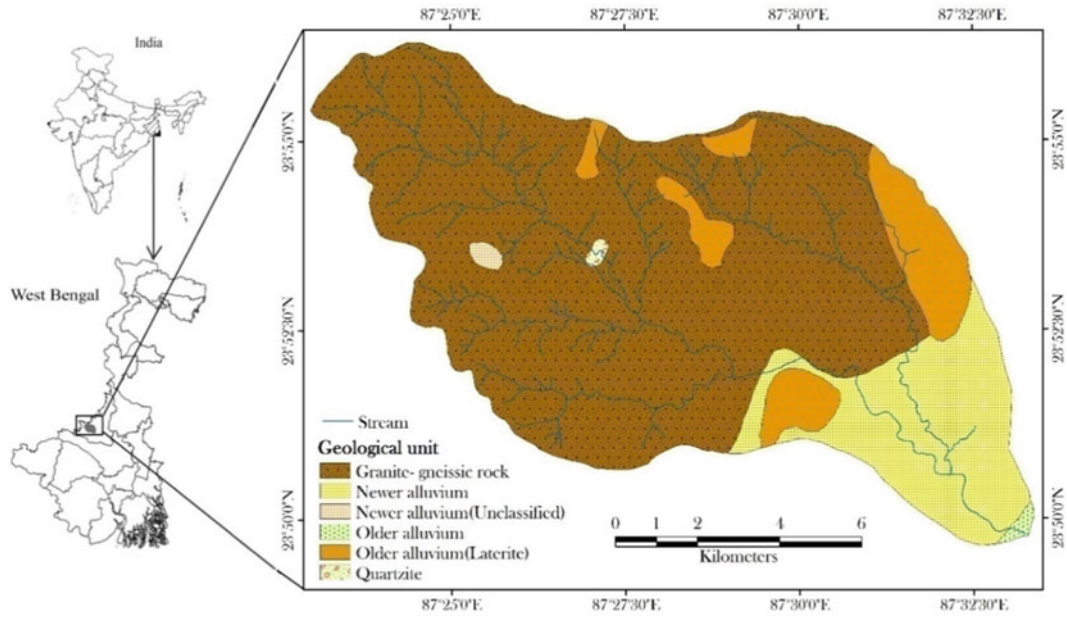

Fig. 14.1 Chandrabhaga river basin showing the geological composition

tropical monsoon with seasonal wet and dry spells of rainfall and cold and hot spells of temperature. The entire year is subdivided into four seasons viz. (1) Winter season (January and February) with low temperature, low humidity level devoid of rain, (2) Pre-monsoon season (March to May) with little rain and high temperature and evaporation, (3) Monsoon season (June to September) with maximum (about 82% of total rain) rain and high temperature and (4) Post-monsoon season (October to November). Average annual rainfall of this basin as gauged by Suri meteorological station is 1444.432 mm. High degree of seasonality of rainfall is reflected by 82% rainfall during the months of June to September (monsoon period).

14.2 Materials and Methods

LANDSAT OLI/TIRS data (path/row: 139/43; spatial resolution 30 m) for 2016 have been obtained from the US Geological Survey (USGS) Global Visualization Viewer and used for deriving land surface temperature (LST), land use/cover (LuLc), evapotranspiration (ET). Monthly spatial rainfall data is extracted from TRMM (Tropical Rainfall Measuring Mission). Although on global scale, the spatial resolution (0.25°) of such multispectral data is considerably high, but for the study of the small-scale hydrological unit, such resolution is still to be considered as coarse (Immerzeel et al. 2009). Duan and Bastiaanssen (2013), Tong et al. (2014) suggested that for downscaling the study, close spacing point data can be created over the study area and inverse distance weighting (IDW) can be adopted for upgrading the spatial scale. Soil texture map of the basin is prepared from the map provided by National Bureau of Soil Survey and Land Use Planning department (India).

14.2.1 Method for Water Balance Calculation

Simple water balance equation (14.1) can be used for predicting regional and seasonal water deficit and surplus (Gokmen et al. 2013; Crosbie et al. 2015). Precipitation, runoff, evaporation, and recharge components are used for this purpose.

$$P = Q + \mathrm{ET_A} + R_{\mathrm{GW}} \tag{14.1}$$

where, P = precipitation; Q = runoff; $\mathrm{ET_A}$ = Actual Evapotranspiration; R_{GW} = Groundwater recharge.

14.2.2 Method for Surface Runoff Estimation

The Soil Conservation Service-Curve Number (SCS-CN) method (USDA) is used for runoff calculation (Eq. 14.2).

$$Q = \frac{(P - I_a)^2}{P - I_a + S} \tag{14.2}$$

where, Q is actual surface runoff in mm, P is rainfall in mm, I_a is 0.4S/0.3S/0.2S/0.1S (season and climatic region-specific) initial abstraction (mm) or losses of water before runoff begins by soil and vegetation (such as infiltration, or rainfall interception by vegetation), 0.3S is usually used for wet, 0.1S is used dry seasons, S is the potential maximum retention. S can be calculated using Eq. 14.3.

$$S = \frac{25,400}{\mathrm{CN}} - 254 \tag{14.3}$$

Some effective parameters for estimating CN for different spatial units are Land use land cover (LULC), hydrological soil group (HSG), and antecedent moisture condition (AMC). LULC map is prepared from multispectral Landsat OLI image following supervised classification (Maximum Likelihood) technique. Accuracy assessment of the classified image is done based on 231 google reference sites and 131 ground base references. Calculated Kappa coefficient of the classified image is 0.93. Arc-CN-Runoff extension tool of ArcGIS is used for precise quantification of runoff. Land use/land cover thematic layer and polygon of soil groups have been used in ARC-CN runoff.

Relative error (RE) (Eq. 14.4) and Nash–Sutcliffe efficiency (NSE) (Eq. 14.5) (Nash and Sutcliffe 1970), are widely used for evaluating the performance of runoff model (Moriasi et al. 2007). This techniqueis used here for testing the model.

$$\mathrm{RE} = \frac{\left(Q_i^{\mathrm{cal}} - Q_i^{\mathrm{obs}}\right)}{\left(Q_i^{\mathrm{obs}}\right)} \times 100\% \tag{14.4}$$

$$\mathrm{NSE} = 1 - \frac{\sum_{i=1}^{n} \left(Q_i^{\mathrm{cal}} - Q_i^{\mathrm{obs}}\right)^2}{\sum_{i=1}^{n} \left(Q_i^{\mathrm{cal}} - Q_{\mathrm{mean}}^{\mathrm{obs}}\right)^2} \tag{14.5}$$

where, Q_i^{obs} = runoff of the ith observation, Q_i^{cal} = calculated runoff of the same observation, $Q_{\mathrm{mean}}^{\mathrm{obs}}$ = mean observed runoff.

RE value nearer to 0 specifies high optimality of the model performances. NSE ranges between $-\infty$ and 1, where NSE = 1 is the optimal result. Values of NSE between 0 and1 are usually assumed as acceptable levels of performance, whereas the value of NSE < 0 points out that the mean observed value is a better predictor than the simulated value, and therefore, is treated as unacceptable (Moriasi et al. 2007). Khatun and Pal (2016) used these testing techniques for assessing the performance level of the runoff model in a similar environment. Actual monthly runoff data is measured at the confluence of Chandrabhaga river at Kaspai for validating models.

14.2.3 Method for Evapotranspiration Estimation

Remote sensing (RS) based Surface Energy Balance Algorithm for Land (SEBAL) is fundamentally used for estimating $\mathrm{ET_A}$. SEBAL utilizes multispectral RS data in corroboration with meteorological data for estimating instantaneous and daily surface energy balance (Eq. 14.6) components (Oliveira et al. 2014). This mechanism produces pixel-to-pixel energy balance information considering the latent heat flux (LE expressed as W m^{-2}). The detail study was made by Bastiaanssen et al. (1998), Silva et al. (2015), and Mahmoud and Alazba (2016).

$$\mathrm{LE} = R_n - G - H \tag{14.6}$$

where, R_n = net radiation (W m^{-2}), G = heat flow in the soil (W m^{-2}), and H = sensible heat flux (W m^{-2}).

The surface albedo (α_s) is worked out from MODIS reflectance data following Trezza et al. (2013) (Eq. 14.7) and the surface emissivity (ε_o) (Eq. 14.8) is articulated based on the LAI (Leaf Area Index) following Allenet al. (2007).

$$\alpha_S = 0.215_{r1} + 0.266_{r2} + 0.242_{r3} + 0.129_{r4} + 0.112_{r6} + 0.036_{r7} \tag{14..7}$$

$$\varepsilon_o = 0.95 + 0.01\mathrm{LAI} \tag{14.8}$$

where, r_1, r_2, r_3, r_4, r_6, and r_7 represent the reflectance spectral bands of the MODIS data.

The LE conversion is calculated from the evaporative fraction (EF), following Bastiaanssen et al. (1998) as presented in Eqs. (14.9) and (14.10). This function supposes that the EF is steady all through the day, but always it may not be as exhibited by Van Niel et al. (2011) and Van Niel et al. (2012). Ruhoff et al. (2012) rightly portrayed that the instant $\mathrm{ET_A}$rate can be acquired as a diurnal average with anticipated inconsistency over outsized scales.

$$\mathrm{EF} = \frac{\mathrm{LE}}{R_n - G} \tag{14.9}$$

$$\mathrm{ET_{AD}} = 0.035\mathrm{EFR}_{n24\mathrm{h}} \tag{14.10}$$

where, $R_{n24\mathrm{h}}$ = net radiation of 24 h calculated from daily solar radiation, surface albedo, and atmospheric transmissivity data, as recommended by Bastiaanssen et al. (1998). Sequentially, the daily actual evapotranspiration is combined along with monthly proportion to the potential evapotranspiration ($\mathrm{ET_P}$), based on the postulation so as to the share between the $\mathrm{ET_{AD}}$ and $\mathrm{ET_P}$ remains equivalent right through the month (Morse et al. 2000) (Eq. 14.11).

$$\mathrm{ET_{AM}} = \frac{\mathrm{ET_{AD}}}{\mathrm{ET_P}} \times \mathrm{ET_{PM}} \tag{14.11}$$

where $\mathrm{ET_{AM}}$ = monthly actual evapotranspiration and $\mathrm{ET_{PM}}$ = monthly cumulative potential evapotranspiration.

For validating ET data derived from satellite data, the empirical formulation can be deployed. Donohue et al. (2010) established that Penman's (1948) equation yields best-fitted result while calculating $\mathrm{ET_P}$ using meteorological data. But based on the ground data available here Blaney–Cridle (1945) method is adopted.

$$\mathrm{ET_{BC}} = P(0.46T + 8.13) \tag{14.12}$$

where $\mathrm{ET_{BC}}$ potential evapotranspiration is in mm/day for a period of consideration. T = mean daily temperature in °C for a period considered = $(T_{\max} + T_{\min})/2$; P = mean daily percentage of total annual daytime hours depending on month and latitude.

14.2.4 Method for Estimation of Recharge

Estimation of groundwater recharge is done from the water balance equation. Positive water balance deducing ET and surface runoff from rainfall can be considered as recharge. Deficit water balance indicates the excess use of soil moisture and soil moisture drought. Groundwater table fluctuation data is one of the sensitive indicators of groundwater recharge. It is assumed that commencing rise of the groundwater table or piezometric surface after rainfall signifies groundwater recharge. So, a simple comparison of monthly estimated recharge from water balance equation and monitoring of the degree and direction of groundwater level fluctuation may help to understand the accuracy level of calculation. Some empirical equations formulated by Chaturvedi (1973), Kumar, and Seetapati (2002) can also be used for calculating recharge and validating the water balance-based recharge data. Recharge volume calculated by the Central Ground Water Board (CGWB) is also taken into consideration for validating the same.

$$R = 2.0(p - 15)^{0.4} \quad (14.13)$$

$$R = 1.2(p - 13)^{0.5} \quad (14.14)$$

where R = groundwater recharge from rainfall during monsoon; p = mean rainfall in monsoon (inch).

14.2.5 Method for Land Surface Temperature Assessment

14.2.5.1 *Conversion of the Digital Number (DN) to Spectral Radiance (Lλ)*

Every object emits thermal electromagnetic energy as its temperature is above absolute zero (K). Following this principle, the signals received by the thermal sensors (ETM+) can be converted to at-sensor radiance. The spectral radiance ($L\lambda$) is calculated using Eq. (14.15) (Landsat Project Science Office 2002).

$$L\lambda = ``\text{gain}'' * \text{QCAL} + ``\text{offset}'' \quad (14.15)$$

where "gain" is the slope of the radiance/DN conversion function; DN is the digital number of a given pixel; bias is the intercept of the radiance/DN conversion function. This is also given as:

$$L\lambda = L_{MIN}\lambda + [\{(L_{\text{MAX}}\lambda - -L_{\text{MIN}}\lambda)/ (\text{QCAL}_{\text{MAX}} - \text{QCAL}_{\text{MIN}})\} * \text{QCAL}] \quad (14.16)$$

where, $\text{QCAL}_{\text{MIN}} = 0$, $\text{QCAL}_{\text{MAX}} = 255$ and QCAL = Digital Number (DN of each pixel).

The $L_{\text{MIN}}\lambda$ and $L_{\text{MAX}}\lambda$ are the spectral radiances for band 6 at digital numbers 0 and 255, respectively. These compute to 3.2 W m^{-2} sr and 12.65 W m^{-2} sr, respectively.

Substitution of the respective values in Eq. (14.16) gives a simpler Eq. (14.17).

$$L\lambda = (0.037059 * \text{DN}) + 3.2 \quad (14.17)$$

14.2.5.2 Conversion of Spectral Radiance (Lλ) to At-Satellite Brightness Temperatures (TB)

Corrections for emissivity (ε) have been applied to the radiant temperatures according to the nature of the land cover. In general, vegetated areas have given a value of 0.95 and non-vegetated areas 0.92 (Nichol 1994). The emissivity corrected surface temperature has been computed following Artis and Carnahan (1982).

$$T_B = \frac{K_2}{\ln\left(\frac{K_1}{L\lambda} + 1\right)} \quad (14.18)$$

where, T_B = At-satellite brightness temperature (K), $L\lambda$ = Spectral Radiance in W m^{-2} sr^{-1} μm^{-1}.

K_1 and K_2 = K_2 and K_1 are two pre-launch calibration constants. (For the Landsat 7 ETM + 6.2 band, these compute to 1282.71 K and 666.09 W m^{-2} sr^{-1} μm, respectively.)

14.2.5.3 Land Surface Temperature (LST)

The obtained temperature values above are referenced to a black body. Therefore, corrections for spectral emissivity (ε) become necessary. These can be done according to the nature of land cover (Snyder et al. 1998) or by deriving corresponding emissivity values from the NDVI values for each pixel. The emissivity corrected land surface temperatures (St) have been computed following Artis and Carnahan (1982).

$$\text{LST} = T_B/[1 + \{(\lambda * TB/\rho) * \ln \varepsilon\}] \quad (14.19)$$

where, LST = Land Surface Temperature (LST) in Kelvin, λ = wavelength of emitted radiance in meters (for which the peak response and the average of the limiting wavelengths (λ = 11.5 μm) (Markham and Barker 1985) is used, $\rho = h*c/\sigma$ (1.438×10^{-2} m K), σ = Boltzmann constant (1.38×10^{-23} J/K), h = Planck's constant (6.626×10^{-34} J s), and c = velocity of light (2.998×10^{8} m/s) and

ε = emissivity (ranges between 0.97 to 0.99). For calculating emissivity of land surface Eq. (14.20) is used.

$$\text{Land surface emissivity } (\varepsilon) = 0.004 * P_{\text{v}} + 0.986 \quad (14.20)$$

where *Pv* is the proportion of vegetation which can be calculated following Eq. (14.21).

$$P_v = \left(\frac{\text{NDVI}_{j_r} - \text{NDVI}_{\min}}{\text{NDVI}_{\max} - \text{NDVI}_{\min}}\right)^2 \quad (14.21)$$

For convenience, the above-derived LSTs' unit is converted to degree Celsius considering the relation between Kelvin and degree Celsius (0 °C = 273.15 K). Degree Celsius data is rather conventional for interpreting the temperature intensity.

For assessing the influences of deficit or surplus water balance patterns on LST, spatial correlation and regression were made.

14.3 Results and Analysis

14.3.1 Rainfall Analysis

Figure 14.2a–l represents the spatial pattern of rainfall in different months of 2016. The annual precipitation data ranges from 1965.06 to 1991.81 mm with insignificant spatial variation in 2016. In the upper and middle catchments during monsoon times the concentration of rainfall is high. Highest rainfall is recorded in monsoon months specifically in July, August, and September. Location of low-pressure axis orients the distribution of rainfall (Fig. 14.2g–i). More than 80% of rainfall is recorded during monsoon months and other months specifically winter and summer months suffer from rainfall scarcity (Table 14.1).

For validating TRMM data, rain gauge data collected from Suri meteorological station is collected and compared. Result states that there is an identical pattern of average rainfall almost in all months (Fig. 14.3a). Only 0.23–21.65% departure of TRMM data from gauge data is recorded and based on this TRMM data can be accepted as representative. Yong et al. (2010), Melo et al. (2015), Coelho et al. (2017) have also applied similar approach for validating TRMM data in the reference data-scarce state.

14.3.2 Runoff Analysis

Figure 14.4a–l represents the spatial sharing of surface runoff in different months of 2016. The maximum runoff volume is recorded at 332.37 mm and 297.11 mm in the month of August and September, respectively (Fig. 14.4h and i) and this high runoff is triggered by enhanced amount of rainfall in that period. Annual average runoff volume for this study area is 51.77 mm. which is 35.227% of average annual rainfall. Out of total annual average runoff, pre-monsoon, monsoon, post-monsoon and winter seasons, respectively carry 6.20%, 69.30%, 22.75%, and 1.75% to total runoff. This information is quite natural in parity with amount of rainfall that happens during these seasons. Spatially this is usually high in the bare lateritic parts of the basin. In few vegetated patches, high runoff is estimated and it is because of very sparse presence of vegetation (Table 14.2).

For testing, the runoff models of different months' Relative error (RE) and Nash–Sutcliffe efficiency (NSE) indices have been used. Result states that RE value ranges from 0.96 to 27% since January to December indicating very less departure of rainfall between estimated and observed runoff. This information validates the spatial runoff models. Average annual NSE value is 0.782 which is near 1 and therefore runoff model can be treated as responsive.

14.3.3 Evapotranspiration Analysis

Figure 14.5a–l illustrates the monthly spatial pattern of evapotranspiration (ET). Annual evapotranspiration state varies from 960.24 to 1074.15 mm/year spatially. In the lower part of the basin, ET is excessively high in monsoon months and quite less in the middle and upper

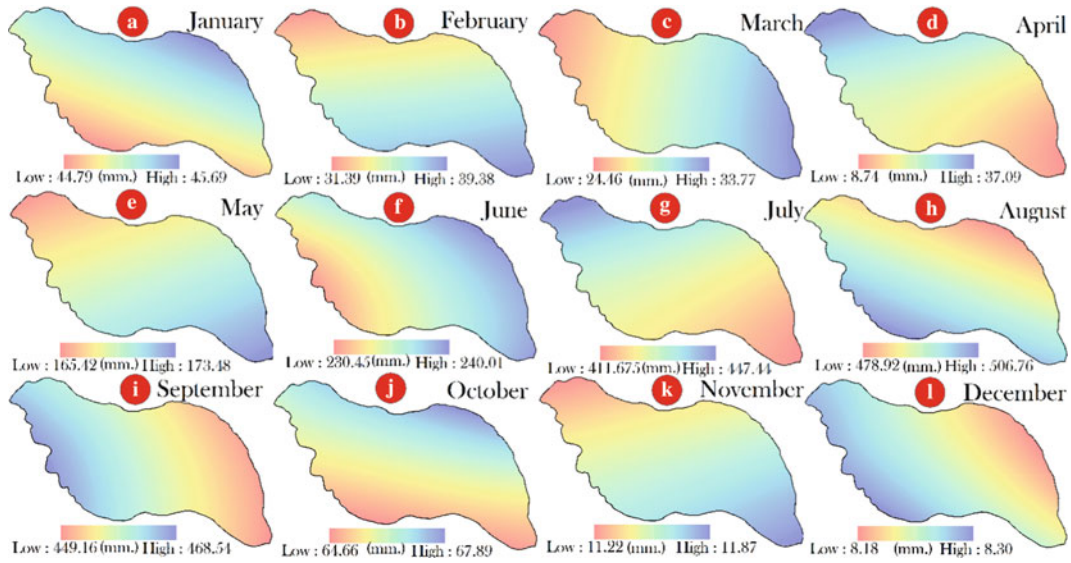

Fig. 14.2 The spatial pattern of rainfall in different months of 2016

part of the basin. Significant seasonal difference in ET is recorded. Highest monthly ET is found in the month of March (138.66 mm) whereas lowest ET (43.73 mm) in the month of December (Table 14.3). Degree of temperature is extremely high during pre-monsoon season, therefore, potential ET is high but actual ET as recorded is not expectedly high. It is because of scarce availability of surface water and soil moisture in this time conditioned by scanty rainfall or no rainfall. In monsoon time, the intensity of temperature is comparatively lower (25–33 °C) than in the pre-monsoon season but due to greater availability of surface water and soil moisture it registers quite greater ET.

Estimated monthly evapotranspiration based on SEBAL method shows a distinct pixel-wise variation in the pattern of ET. The variation of ET for different land covers shows the hourly ET ranged from 0 at bareland and rock outcrops to 0.504 mm per hour in forest areas and the daily ET varies from 0.0 to 12.09 mm per day at the same land cover classes. The mainland covers controlling the ET characteristics is the vegetated land which scatteredly covers about 20.38% of the study area. The least range of variation in the hourly ET values appears in the bare land area indicating absence of vegetation cover. The results show a clear relation between land use/land cover and solar radiation parameters and impact of vegetation cover on the ET values in pixel domain.

Figure 14.3b represents the scatter plot of atmospheric ET and calculated ET for different months of 2016. This regression graph is plotted for showing validity of calculated ET models. Monthly ET data was collected from Suri gauge station for this purpose. Strong coefficient of determination (R^2) value (0.8561) and correlation coefficient (0.785) establish the validity of ET models.

14.3.4 Groundwater Recharge/Deficit

Using water balance method, estimation of monthly groundwater recharge for the year 2016 was done. Average annual recharge is 356.386 mm with significant seasonal and intra-seasonal monthly variation. Highest estimated recharge is recorded in the months of July, August, and September (Table 14.4), and these amounts are

Table 14.1 Average, minimum, and maximum monthly rainfall of Chandrabhaga river basin with descriptive statistics

Months	January	February	March	April	May	June	July	August	September	October	November	December
Min. (mm)	44.79	31.39	24.46	8.74	165.42	230.45	411.68	478.92	449.16	64.67	11.22	8.18
Max. (mm)	45.69	39.38	33.77	34.10	173.49	240.01	447.44	506.77	468.54	67.89	11.87	8.30
Mean (mm)	45.24	35.62	39.30	22.24	169.51	235.82	426.44	492.97	458.28	66.07	11.55	8.24
SD	0.20	1.75	2.35	5.98	1.71	2.28	7.71	6.18	5.03	0.74	0.14	0.03
CV(%)	0.44	4.90	5.97	26.89	1.01	0.97	1.81	1.25	1.10	1.12	1.19	0.33

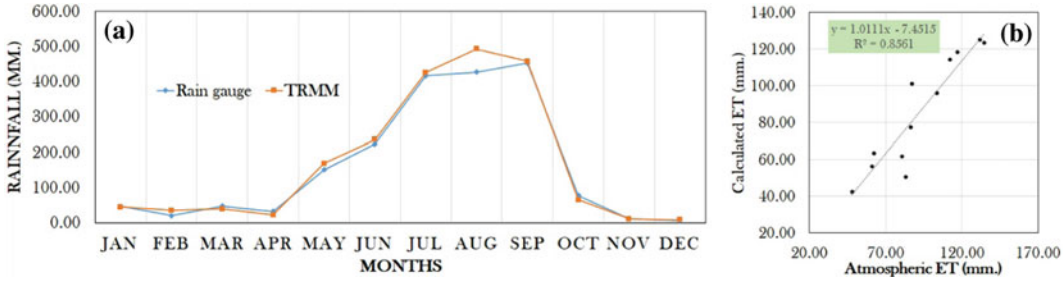

Fig. 14.3 **a** Comparision of monthly average rainfall data collected from TRMM data and gauge data; **b** regression pattern between monthly average observed and calculated ET

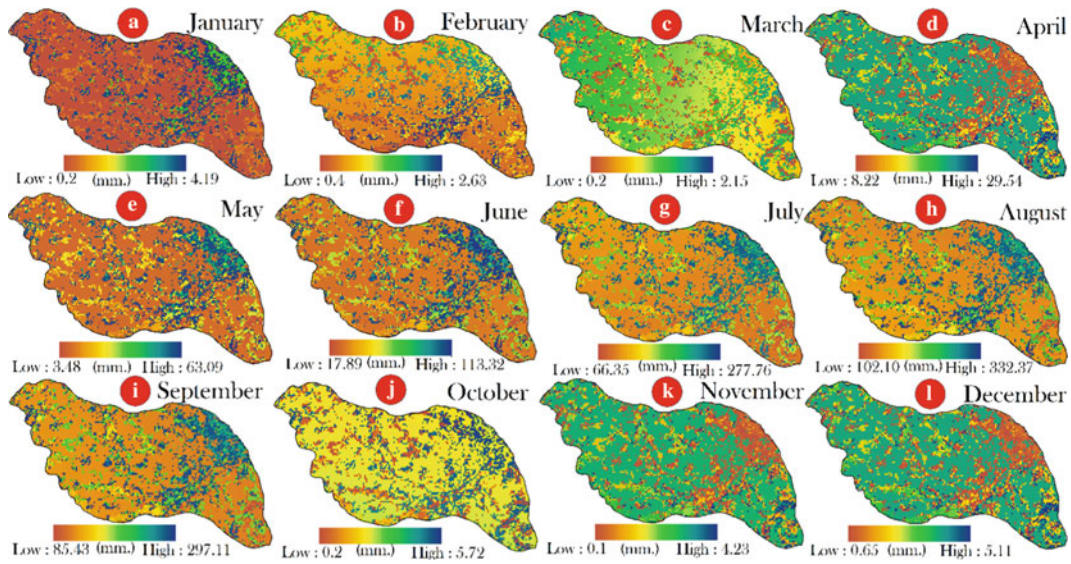

Fig. 14.4 Monthly spatial pattern of estimated surface runoff in Chandrabhaga river basin

44.36, 41.38, and 50.89% of the rainfall, respectively, as extracted from TRMM data. These recharges are the principle source of groundwater in this region. Negative water balance is recorded in winter and summer months indicating seasonal drought. Seasonal soil moisture deficit disrupts agricultural activities in these seasons. Excessive groundwater withdrawal for agriculture and other domestic and commercial uses makes drought states more prominent. Water deficit state is very explicit in the upper and middle catchments of the basin (Fig. 14.6b–d, k, l). Coarser soils with very little moisture retaining capacity, and excess ET are responsible for such stress state of moisture deficit. Poor soil moisture (<7%) in this area also supports this state. Groundwater recharge and rise of water table are well explained by recorded groundwater level data collected from Central Ground Water

Table 14.2 Average, minimum, and maximum monthly surface runoff of Chandrabhaga river basin with descriptive statistics

Months	January	February	March	April	May	June	July	August	September	October	November	December
Min.(mm)	0.20	0.40	0.20	8.22	3.48	17.90	66.35	102.10	85.43	0.20	0.10	0.65
Max. (mm)	4.19	2.63	2.15	29.55	63.09	113.32	277.76	332.37	297.11	5.72	4.23	5.11
Mean (mm)	1.89	1.64	0.78	20.16	21.29	49.61	140.49	187.13	162.31	2.58	2.31	3.11
SD	1.51	0.61	0.38	6.70	19.91	31.55	62.52	69.94	65.94	1.56	1.25	1.41
CV(%)	80.28	37.19	49.17	33.22	93.49	63.60	44.51	37.37	40.63	60.37	54.10	45.19

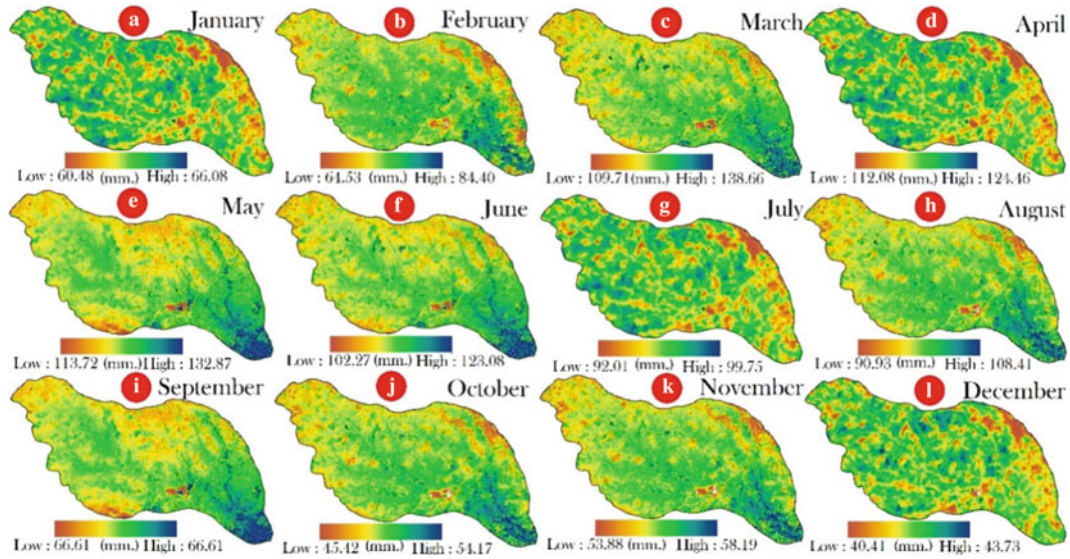

Fig. 14.5 Monthly spatial pattern of estimated ET in Chandrabhaga river basin

Board and State Water Investigation Directorate. Groundwater level during monsoon months is 5 m below ground surface.

14.3.5 Temporal Pattern of Water Balance

Finally, from all these models of water balance components, monthly water balance equations are derived (Table 14.5). January, February, March, April, May, November, and December are appeared as water deficit (negative water balance) months and rest five months are emerged as water surplus (positive water balance) months. Annual water balance states that 15.47% of area falls under water deficit and 84.53% underwater surplus. Calculation of net water balance would result in positive water balance. But, seasonal water deficit cannot be overlooked. Seasonal water deficit not only withstands against agricultural productivity in the densely populated and demanding areas but it can aggravate the temperature condition of the deficit region. Prominent soil cracking, lowering of groundwater level, drying out of ponds and wetlands are some of the evidences for such seasonal water deficit conditions.

14.3.6 Land Surface Temperature

The spatial distribution of LST in different months of 2016 is shown in Fig. 14.7. In winter season, LST ranges from 19.59 to 23.85 °C (mean 22.41 °C), pre-monsoon season temperature ranges from 23.97 to 41.43 °C (mean 35.83 °C) and in monsoon season temperature is confined within 19.74–33.23 °C (mean 26.79 °C) (Table 14.6). High temperature is registered in the upper part of the basin where lateritic bare soil predominates. Temperature regime is not only associated with incoming solar radiation but also strongly linked with land use/cover (Pal and Ziaul 2017; Ziaul and Pal 2016; Fu and Weng 2016; Feng et al. 2014). Green spaces and

Table 14.3 Average, minimum, and maximum monthly ET of Chandrabhaga river basin with descriptive statistics

Months	January	February	March	April	May	June	July	August	September	October	November	December
Min. (mm)	60.48	64.53	109.71	112.08	113.72	102.27	92.01	90.93	57.03	45.42	53.88	40.40
Max. (mm)	66.08	84.40	138.66	124.46	132.87	123.09	99.75	108.41	66.61	54.17	58.20	43.73
Mean (mm)	63.33	77.30	125.17	118.42	123.42	114.30	95.98	101.25	61.89	50.59	56.46	42.43
SD	0.85	1.06	1.32	1.92	1.10	1.14	1.19	1.05	0.55	0.52	0.25	0.44
CV(%)	1.34	1.38	1.05	1.62	0.89	1.00	1.24	1.04	0.89	1.04	0.45	1.04

Table 14.4 Average, minimum, and maximum monthly water balance (surplus or deficit states) of Chandrabhaga river basin with descriptive statistics

Months	January	February	March	April	May	June	July	August	September	October	November	December
Min. (mm)	−23.96	−48.37	−105.23	−150.60	−18.83	7.45	68.60	66.49	105.15	6.59	−49.94	−41.68
Max. (mm)	−15.42	−30.53	−84.03	−119.67	47.71	109.48	268.61	288.29	310.81	19.24	−43.27	−34.67
Mean (mm)	−19.02	−42.37	−96.74	−137.35	24.49	71.49	189.21	204.00	233.24	12.85	−47.25	−38.88
SD	1.40	1.75	2.27	7.79	19.83	31.03	62.29	70.61	66.84	1.78	1.33	1.65
CV(%)	−7.36	−4.12	−2.34	−5.67	80.98	43.40	32.92	34.61	28.66	13.86	−2.81	−4.25

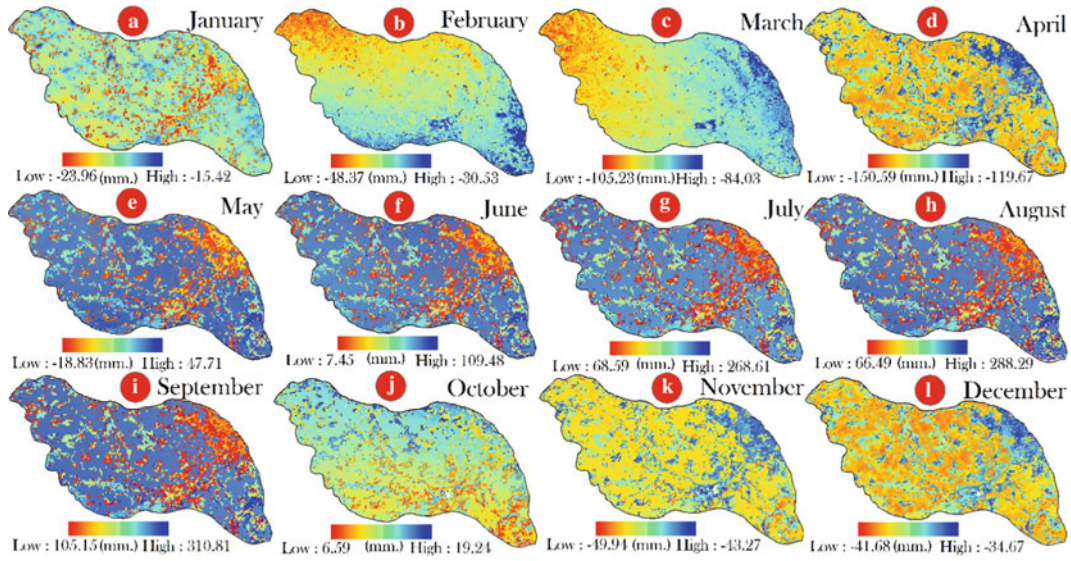

Fig. 14.6 Water deficit and surplus states calculated from water balance equation in different months in 2016

Table 14.5 Mean water balance component values and water balance equation; value within parenthesis indicates the ratio between the hydrological component and ppt

Months	Rainfall	Runoff	ET	Recharge	Water balance equation	Remarks
January	45.24	1.89	24.20	10.12	$P_{45.24} = Q^{0.04} + \mathrm{ET}^{1.40} + R^{-0.42}$	Recharge negative
February	35.62	1.64	15.63	14.97	$P_{35.62} = Q^{0.05} + \mathrm{ET}^{2.17} + R^{-1.19}$	Recharge negative
March	39.30	0.78	114.95	–86.51	$P_{39.30} = Q^{0.02} + \mathrm{ET}^{3.18} + R^{-2.46}$	Recharge negative
April	22.24	20.16	90.82	–110.86	$P_{22.24} = Q^{0.91} + \mathrm{ET}^{5.32} + R^{-6.18}$	Recharge negative
May	169.51	21.29	123.00	24.97	$P_{169.51} = Q^{0.13} + \mathrm{ET}^{0.73} + R^{0.14}$	Recharge positive
June	235.82	49.61	91.21	110.14	$P_{235.82} = Q^{0.21} + \mathrm{ET}^{0.48} + R^{0.30}$	Recharge positive
July	426.44	140.49	203.72	111.11	$P_{426.44} = Q^{0.33} + \mathrm{ET}^{0.23} + R^{0.44}$	Recharge positive
August	492.97	187.13	214.00	145.97	$P_{492.97} = Q^{0.38} + \mathrm{ET}^{0.21} + R^{0.41}$	Recharge positive
September	458.28	162.31	198.94	138.60	$P_{458.28} = Q^{0.35} + \mathrm{ET}^{0.14} + R^{0.51}$	Recharge positive
October	66.07	2.58	43.23	20.20	$P_{66.07} = Q^{0.04} + \mathrm{ET}^{0.77} + R^{0.19}$	Recharge positive
November	11.55	2.31	5.28	3.94	$P_{11.55} = Q^{0.20} + \mathrm{ET}^{4.89} + R^{-4.09}$	Recharge negative
December	8.24	3.11	2.65	0.92	$P_{8.24} = Q^{0.38} + \mathrm{ET}^{5.15} + R^{-4.72}$	Recharge negative

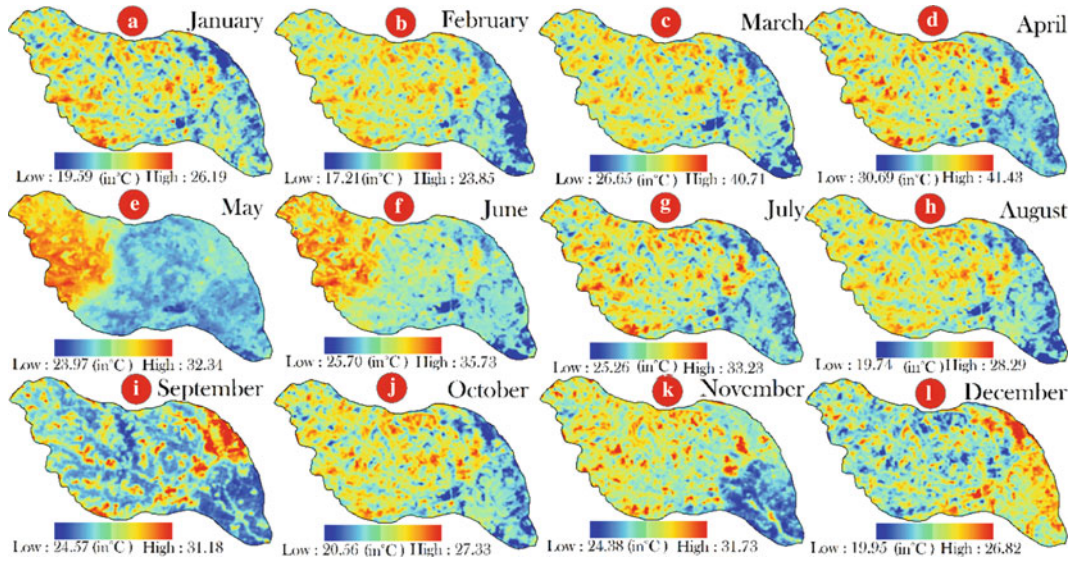

Fig. 14.7 **a–l** Monthly spatial LST, 2016 in Chandrabhaga river basin

adjacency of water bodies lead to low-temperature state but bare soil portion of the study area recorded high temperature.

14.3.7 Spatial Association Between LST and Water Deficit

In this section, it is tried to investigate is water deficit area of the study area sensitive to high temperature and reverse in the surplus area. Pixel-based spatial correlation states that although the relation is not so strong but such relation prevails thereon. Correlation coefficient between water deficit intensity and degree of LST is −0.2366 and this value is also significant at 0.05 level of confidence. Water deficit area also experiences strong ET as indicated by significant *r* value (−0.6748). So, along with other factors, water deficit can also be treated as one of the causes of relatively greater LST in some parts of the basin. On the contrary, when surplus water balance pixels are related to LST of the concerned pixels, it is found that the pixels having greater surplus water balance possess lesser temperature and vice versa (Fig. 14.8).

14.4 Conclusion

The present work tried to establish the influence of seasonal and regional water deficit states on enhanced LST and water surplus states on relatively less temperatures. For doing this monthly water balance equations are derived and mapped out spatial scale on the one hand and monthly land surface temperature is estimated and mapped out on the other hand. Finally, spatial associateship is analyzed quantitatively. From the result, it is clearly found that seven months (January to May, November, and December) are identified as water deficit months (up to −150.59 mm), and five months (June to October) are recognized as water surplus months (Highest 310.81 mm). In the deficit months, upper and middle catchments are prone to water deficit. Bare coarse-grain laterite soil also triggers high temperature. LST is also correlation coefficient between water deficit and LST is −0.2366 and it is 0.1785 between water surplus and LST and these are significant at 0.05 level of significance. So, spatial and seasonal water balance state can be treated as one of the reasons for degree of temperature distribution over the study area.

Table 14.6 Average, minimum, and maximum monthly Surface temperature of Chandrabhaga river basin with descriptive statistics

Months	January	February	March	April	May	June	July	August	September	October	November	December
Min. (°C)	19.59	17.21	26.65	30.69	23.97	25.70	25.26	19.74	24.57	20.56	24.38	19.95
Max. (°C)	26.19	23.85	40.71	41.43	32.34	35.73	33.23	28.29	31.18	27.33	31.73	26.82
Mean (°C)	22.56	20.97	35.39	35.54	27.56	31.48	29.05	25.09	25.99	24.39	26.97	23.71
SD	0.96	1.16	1.84	1.79	1.91	1.52	1.33	1.28	0.81	1.06	1.06	0.91
CV(%)	4.25	5.53	5.20	5.03	6.92	4.83	4.58	5.10	3.12	4.35	3.92	3.86

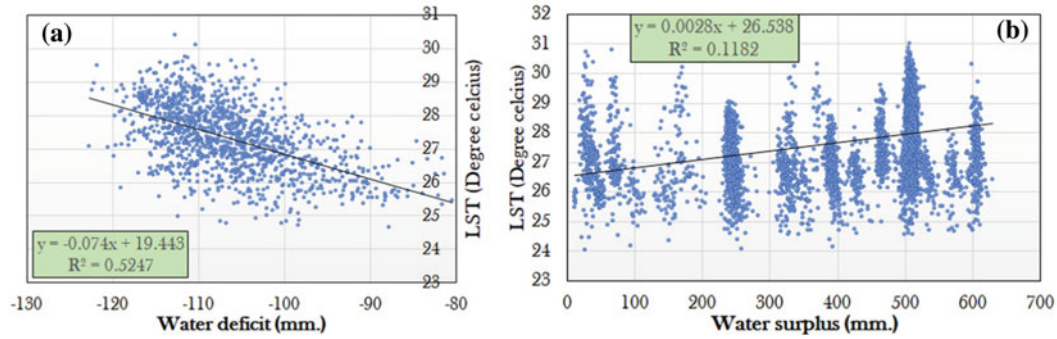

Fig. 14.8 **a**, **b** Correlation between LST and water deficit pixels and water surplus pixels

Funding The first author of the article would like to thank University Grants Commission (UGC Ref. No. 3379/(OBC)(NET-NOV 2017), New Delhi, India for providing financial support as junior research fellowship to conduct the research work presented in this paper.

References

Allen RG, Tasumi M, Morse A, Trezza R, Wright JL, Bastiaanssen W, Kramber W, Lorite I, Robison CW (2007) Satellite-based energy balance for mapping evapotranspiration with internalized calibration (METRIC)—applications. J Irrig Drain Eng 133:395–406. https://doi.org/10.1061/(ASCE)0733-9437(2007)133:4(395)

Artis DA, Carnahan WH (1982) Survey of emissivity variability in thermography of urban areas. Remote Sens Environ 12:313–329

Bagchi K, Mukerjee KN (1983) Diagnostic survey of West Bengal(s). Dept. of Geography, Calcutta University, Pantg Delta & Rarh Bengal

Bastiaanssen WGM, Menenti M, Feddes RA, Holtslag AAM (1998) A remote sensing surface energy balance algorithm for land (SEBAL). 1. Formulation. J Hydrol 212:198–212

Bastiaanssen WGM, Noordman EJM, Pelgrum H, Davids G, Thoreson BP, Allen RG (2005) SEBAL model with remotely sensed data to improve water-resources management under actual field conditions. J Irrig Drain Eng 131(1):85–93

Blaney HF, Criddle WD (1945) Determining water requirements in irrigated areas from climatological data. Processed 17

Chaturvedi RS (1973) A note on the investigation of ground water resources in western districts of Uttar Pradesh. Annual Report, U.P. Irrigation Research Institute, pp 86–122

Coelho VHR, Montenegro S, Almeida CN, Silva BB, Oliveira LM, Gusmão ACV, Freitas ES, Montenegro AAA (2017) Alluvial groundwater recharge estimation in semi-arid environment using remotely sensed data. J Hydrol. https://doi.org/10.1016/j.jhydrol.2017.02.054

Crosbie RS, Davies P, Harrington N, Lamontagne S (2015) Ground trothing groundwater-recharge estimates derived from remotely sensed evapotranspiration: a case in South Australia. Hydrogeol J 23:335–350. https://doi.org/10.1007/s10040-014-1200-7

Deo RC, Şahin M (2017) Forecasting long-term global solar radiation with an ANN algorithm coupled with satellite-derived (MODIS) land surface temperature (LST) for regional locations in Queensland. Renew Sustain Energy Rev 72:828–848

Donohue RJ, McVicar TR, Roderick ML (2010) Assessing the ability of potential evaporation formulations to capture the dynamics in evaporative demand within a changing climate. J Hydrol 386:186–197. https://doi.org/10.1016/j.jhydrol.2010.03.020

Duan Z, Bastiaanssen WGM (2013) First results from Version 7 TRMM 3B43 precipitation product in combination with a new downscaling–calibration procedure. Remote Sens Environ 131:1–13

Feng H, Zhao X, Chen F, Wu L (2014) Using land use change trajectories to quantify the effects of urbanization on urban heat island. Adv Space Res 53(3):463–473

Fu P, Weng Q (2016) A time series analysis of urbanization induced land use and land cover change and its impact on land surface temperature with Landsat imagery. Remote Sens Environ 175:205–214

Gokmen M, Vekerdy Z, Lubczynski MW, Timmermans J (2013) Assessing groundwater storage changes using remote sensing-based evapotranspiration and precipitation at a large semiarid basin scale. J Hydrometeorol 16:129–146. https://doi.org/10.1175/JHM-D-12-0156.1

González GM, Stisen S, Koch J (2015) Retrieval of spatially distributed hydrological properties based on surface temperature rise measured from space for spatial model validation at regional scale

González-Rojí SJ, Sáenz J, Ibarra-Berastegi G, Díaz de Argandoña J (2018) Moisture balance over the Iberian Peninsula according to a regional climate model. The

impact of 3DVAR data assimilation. J Geophys Res: Atmos

Hassan-Esfahani L, Torres-Rua A, McKee M (2015) Assessment of optimal irrigation water allocation for pressurized irrigation system using water balance approach, learning machines, and remotely sensed data. Agric Water Manag 153:42–50

Hu P, Liu Q, Heslop D, Roberts AP, Jin C (2015) Soil moisture balance and magnetic enhancement in loess–paleosol sequences from the Tibetan Plateau and Chinese Loess Plateau. Earth Planet Sci Lett 409:120–132

Immerzeel WW, Droogers P, De Jong SM, Bierkens MFP (2009) Large-scale monitoring of snow cover and runoff simulation in Himalayan river basins using remote sensing. Remote Sens Environ 113(1):40–49

Jafari R, Hasheminasab S (2017) Assessing the effects of dam building on land degradation in central Iran with Landsat LST and LULC time series. Environ Monit Assess 189(2):74

Jha AK (2013) Water availability, scarcity and climate change in India: a review. Asian J Water Environ 1 (1):50–66

Jiang Y, Weng Q (2017) Estimation of hourly and daily evapotranspiration and soil moisture using down-scaled LST over various urban surfaces. Giscience Remote Sens 54(1):95–117

Khalaf A, Donoghue D (2012) Estimating recharge distribution using remote sensing: a case study from the West Bank. J Hydrol 414:354–363

Khatun S, Pal S (2016) Identification of prospective surface water available zones with multi criteria decision approach in Kushkarani river basin of eastern India. Arch Curr Res Int 4(4):1–20

Krol MS, Bronstert A (2007) Regional integrated modelling of climate change impacts on natural resources and resource usage in semi-arid Northeast Brazil. Environ Model Softw 22(2):259–268

Kumar CP, Seetapati PV (2002) Assessment of natural ground water recharge in upper Ganga canal command area. J Appl Hydrol 15(4):13–20

Landsat Project Science Office (2002) Landsat 7 science data user's handbook. Goddard Space Flight Center, NASA, Washington, DC. http://ltpwww.gsfc.nasa.gov/IAS/hand-book/handbook_toc.html. Accessed 10 Sept 2003

Lee TW, Lee JY, Wang ZH (2012) Scaling of the urban heat island intensity using time-dependent energy balance. Urban Climate 2:16–24

Mahmoud SH, Alazba AA (2016) A coupled remote sensing and the Surface Energy Balance based algorithms to estimate actual evapotranspiration over the western and southern regions of South Arabia. J Asian Earth Sci 124:269–283. https://doi.org/10.1016/j.jseaes.2016.05.012

Markham BL, Barker JL (1985) Spectral characterization of the Landsat thematic mapper sensors. Int J Remote Sens 6(5):697–716

Meena AL, Bisht P (2017) Study of variability of rainfall and suitability of farming in sub-humid region: a case study of Jaipur District, Rajasthan, India. Sustain Agri Food Environ Res 5(3)

Melo DCD, Xavier AC, Bianchi T, Oliveira PTS, Scanlon B, Lucas MC, Wendland E (2015) Performance and evaluation of rainfall estimates by TRMM multi-satellite precipitation analysis 3B42V6 and V7 over Brazil. J Geophys Res 120:9426–9436. https://doi.org/10.1002/2015JD023797

Metz M, Andreo V, Neteler M (2017) A new fully gap-free time series of land surface temperature from MODIS LST data. Remote Sens 9(12):1333

Mishra V, Shah R, Thrasher B (2014) Soil moisture droughts under the retrospective and projected climate in India. J Hydrometeorol 15(6):2267–2292

Mohanty BP, Ines AV, Shin Y, Gaur N, Das N, Jana R (2017) A framework for assessing soil moisture deficit and crop water stress at multiple space and time scales under climate change scenarios using model platform, satellite remote sensing, and decision support system. In: Remote sensing of hydrological extremes. Springer, Cham, pp 173–196

Mooley DA, Parthasarathy B (1984) Fluctuations in all India summer monsoon rainfall during 1871–1978. Clim Change 6:287–301

Moriasi DN, Arnold JG, Van Liew MW, Bingner RL, Harmel RD, Veith TL (2007) Model evaluation guidelines for systematic quantification of accuracy in watershed simulations. Trans ASABE 50(3):885–900

Morse A, Allen RG, Tasumi M, Kramber WJ, Trezza R, Wright J (2000) Application of the SEBAL methodology for estimating evapotranspiration and consumptive use of water through remote sensing. University of Idaho, Kimberly, ID, USA, pp 1–220

Nash JE, Sutcliffe JV (1970) River flow forecasting through conceptual models. Part I. A discussion of principles. J Hydrol 10(3):282–290

Nichol JE (1994) A GIS-based approach to microclimate monitoring in Singapore's highrise housing estates. Photogramm Eng Remote Sens 60:1225–1232

Oliveira LMM, Montenegro SMGL, Silva BB, Antonino ACD, Moura AESS (2014) Evapotranspiração real em bacia hidrográfica do Nordeste brasileiro por meio do SEBAL e produtos MODIS. Rev Bras Eng Agríc Ambient 18:1039–1046. https://doi.org/10.1590/1807-1929/agriambi.v18n10p1039-1046

Pal S, Ziaul S (2017) Detection of land use and land cover change and land surface temperature in English Bazar urban centre. Egypt J Remote Sens Space Sci 20 (1):125–145

Penman HL (1948) Natural evaporation from open water, bare soil and grass. Proc R Soc London A193:120–145. https://doi.org/10.1098/rspa.1948.0037

Perea RG, Poyato EC, Montesinos P, Morillo JG, Díaz JR (2016) Influence of spatio temporal scales in crop water footprinting and water use management: evidences from sugar beet production in Northern Spain. J Clean Prod 139:1485–1495

Rohde MM, Edmunds WM, Freyberg D, Sharma OP, Sharma A (2015) Estimating aquifer recharge in fractured hard rock: analysis of the methodological

challenges and application to obtain a water balance (Jaisamand Lake Basin, India). Hydrogeol J 23 (7):1573–1586

Ruhoff AL, Paz AR, Collischonn W, Aragão LEOC, Rocha HR, Malhi YS (2012) A MODIS-based energy balance to estimate evapotranspiration for clear-sky days in Brazilian Tropical Savannas. Remote Sens 4:703–725. https://doi.org/10.3390/rs4030703

Saiter FZ, Eisenlohr PV, Barbosa MR, Thomas WW, Oliveira-Filho AT (2016) From evergreen to deciduous tropical forests: how energy–water balance, temperature, and space influence the tree species composition in a high diversity region. Plant Ecolog Divers 9(1):45–54

Sathyanadh A, Karipot A, Ranalkar M, Prabhakaran T (2016) Evaluation of soil moisture data products over Indian region and analysis of spatio-temporal characteristics with respect to monsoon rainfall. J Hydrol 542:47–62

Shao HB, Chu LY, Jaleel CA, Manivannan P, Panneerselvam R, Shao MA (2009) Understanding water deficit stress-induced changes in the basic metabolism of higher plants–biotechnologically and sustainably improving agriculture and the ecoenvironment in arid regions of the globe. Crit Rev Biotechnol 29(2):131–151

Shiklomanov IA (2000) Appraisal and assessment of world water resources. Water Int 25(1):11–32

Silva BB, Wilcox BP, Silva VPR, Montenegro SMGL, Oliveira LMM (2015) Changes to the energy budget and evapotranspiration following conversion of tropical savannas to agricultural lands in São Paulo State, Brazil. Ecohydrology 8:1272–1283. https://doi.org/10.1002/eco.1580

Siu LW, Hart MA (2013) Quantifying urban heat island intensity in Hong Kong SAR, China. Environ Monit Assess 185(5):4383–4398

Snyder WC, Wan Z, Zhang Y, Feng YZ (1998) Classification-based emissivity for land surface temperature measurement from space. Int J Remote Sens 19(14):2753–2774

Surendran S, Gadgil S, Francis PA, Rajeevan M (2015) Prediction of Indian rainfall during the summer monsoon season on the basis of links with equatorial Pacific and Indian Ocean climate indices. Environ Res Lett 10(9):094004

Thober S, Kumar R, Sheffield J, Mai J, Schäfer D, Samaniego L (2015) Seasonal soil moisture drought prediction over Europe using the North American Multi-Model Ensemble (NMME). J Hydrometeorol 16 (6):2329–2344

Tong K, Su F, Yang D, Hao Z (2014) Evaluation of satellite precipitation retrievals and their potential utilities in hydrologic modeling over the Tibetan Plateau. J Hydrol 519:423–437. https://doi.org/10.1016/j.jhydrol.2014.07.044

Trezza R, Allen RG, Tasumi M (2013) Estimation of actual evapotranspiration along the Middle Rio Grande of New Mexico using MODIS and Landsat Imagery with the METRIC Model. Remote Sens 5:5397–5423. https://doi.org/10.3390/rs5105397

Van Niel TG, McVicar TR, Roderick ML, van Dijk AIJM, Renzullo LJ, van Gorsel E (2011) Correcting for systematic error in satellite-derived latent heat flux due to assumptions in temporal scaling: assessment form flux tower observations. J Hydrol 409:140–148. https://doi.org/10.1016/j.jhydrol.2011.08.011

Van Niel TG, McVicar TR, Roderick ML, van Dijk AIJM, Beringer J, Hutley LB, van Gorsel E (2012) Upscaling latent heat flux for thermal remote sensing studies: comparison of alternative approaches and correction of bias. J Hydrol 468–469:35–46. https://doi.org/10.1016/j.jhydrol.2012.08.005

Vero SE, Antille DL, Lalor STJ, Holden NM (2014) Field evaluation of soil moisture deficit thresholds for limits to trafficability with slurry spreading equipment on grassland. Soil Use Manag 30(1):69–77

Wada Y, Beek LP, Sperna Weiland FC, Chao BF, Wu YH, Bierkens MF (2012) Past and future contribution of global groundwater depletion to sea-level rise. Geophys Res Lett 39(9)

Yadav SS, Lal R (2018) Vulnerability of women to climate change in arid and semi-arid regions: the case of India and South Asia. J Arid Environ 149:4–17

Yaduvanshi A, Ranade A (2017) Long-term rainfall variability in the eastern Gangetic plain in relation to global temperature change. Atmos Ocean 55(2):94–109

Yao R, Wang L, Huang X, Niu Y, Chen Y, Niu Z (2018) The influence of different data and method on estimating the surface urban heat island intensity. Ecol Ind 89:45–55

Yong B, Ren L, Hong Y, Wang J, Gourley JJ, Jiang SH, Chen X, Wang W (2010) Hydrologic evaluation of Multisatellite Precipitation Analysis standard precipitation products in basins beyond its inclined latitude band: a case study in Laohahe basin, China. Water Resour Res 46:1–20. https://doi.org/10.1029/2009WR008965

Zandalinas SI, Balfagón D, Arbona V, Gómez-Cadenas A, Inupakutika MA, Mittler R (2016) ABA is required for the accumulation of APX1 and MBF1c during a combination of water deficit and heat stress. J Exp Bot 67(18):5381–5390

Zhang X, Tang Q, Liu X, Leng G, Li Z (2017) Soil moisture drought monitoring and forecasting using satellite and climate model data over Southwestern China. J Hydrometeorol 18(1):5–23

Ziaul S, Pal S (2016) Image based surface temperature extraction and trend detection in an urban area of West Bengal, India. J Environ Geogr 9(3–4):13–25